Effects of two-temperature model on cascade evolution in Ni and NiFe

Eva Zarkadoula,[1] German Samolyuk,[1] Haizhou Xue,[2] Hongbin Bei,[1] and William J. Weber[2, 1]

[1]*Materials Science & Technology Division, Oak Ridge National Laboratory, Oak Ridge, TN 37831, USA*
[2]*Department of Materials Science & Engineering, University of Tennessee, Knoxville, TN 37996, USA*

We perform molecular dynamics simulations of Ni ion cascades in Ni and equiatomic NiFe under the following conditions: (a) classical molecular dynamics (MD) simulations without consideration of electronic energy loss, (b) classical MD simulations with the electronic stopping included, and (c) using the coupled two-temperature MD (2T-MD) model that incorporates both the electronic stopping and the electron-phonon interactions. Our results indicate that the electronic effects are more profound in the higher energy cascades and that the 2T-MD model results in a smaller amount of surviving damage and smaller defect clusters, while less damage is produced in NiFe than in Ni.

When fast ions are moving through matter, part of their energy is lost due to elastic nuclear collisions (i.e., ballistic processes), while the remaining energy is lost due to their interaction with the electrons of the target material. Numerous studies [1–4] have focused on radiation effects in matter due to ballistic processes only; however, the effects of kinetic energy transferred to the electrons on the materials' behavior under irradiation are not well understood.

Recent molecular dynamics (MD) simulations of radiation effects have highlighted the significance of the electronic excitations in the evolution of high-energy cascades (100 – 500 keV) in monoatomic metals [5–7], where the electronic processes affect the level of the surviving damage and the defect cluster distribution. Additionally, while the electronic effects are dominant in high energy events, their importance in lower energy radiation events is yet to be investigated. In the present study we investigate the effects of electronic excitations for lower energy cascades in Ni and equiatomic NiFe.

Nickel based high entropy alloys are candidate structural materials of next generation fusion reactors due to their good mechanical, thermal, electric and magnetic properties [8–14]. NiFe is a single-phase concentrated solid-solution with the same structure as Ni (fcc). We provide a comparison of the damage produced in each material without and with the electronic effects included in the simulations of 30 and 50 keV Ni ion cascades.

We use the MD code DLPOLY [15] v.4.04, where the 2T-MD model according to Duffy and Rutherford model [16, 17] is incorporated. For each system we perform simulations under three different conditions: a) classical MD cascade simulations, b) classical cascade simulations with the electronic stopping mechanism activated as a friction term, which we will call friction cascades, and (c) cascades where the full two-temperature (2T-MD) model is implemented, i.e. the electron-phonon interaction is taken into account in addition to the electronic stopping. In the friction cascades, the electronic stopping is included in the equation of motion as a friction term. In the 2T-MD cascades the friction term has one more component which corresponds to the electron-phonon (e-ph) interactions. Additionally, energy lost by the friction term is fed back to the system via the e-ph coupling. The evolution of the electronic energy is described by a heat diffusion equation, which is solved using a finite difference method, and it is coupled to the MD simulation via a Langevin thermostat. This way the excess energy is transported from the simulation cell via electronic thermal conduction and the heat transport in the cascade is included. More details can be found elsewhere [6].

We performed 30 keV and 50 keV Ni ion cascade simulations of twelve randomly chosen directions of the primary knock-on atom (PKA) for each energy at 300 K, in systems consisting of 2.5 and 3.6 million atoms with MD box lengths of about 305 and 345 Å respectively. A thermostat of 8 Å width is applied at the MD box boundaries, where the atom velocities are rescaled according to a Gaussian distribution to correspond to the target temperature and emulate the energy dissipation into the sample. Alternatively, the use of a Langevin boundary thermostat, offering a natural way to scale the excess energy at the MD box boundaries, has been also suggested [18] for nonequilibrium dynamics. We are using an embedded-atom (EAM) potential of Bonny et al [19] that was developed to model point defects in Ni-Fe-Cr systems. The systems are equilibrated under the constant pressure and temperature ensemble (NPT) prior to irradiation, using a Berendsen thermostat and barostat and a constant timestep of 1 fs. For the cascade simulations a variable timestep is used to describe the atomic motion throughout the irradiation process.

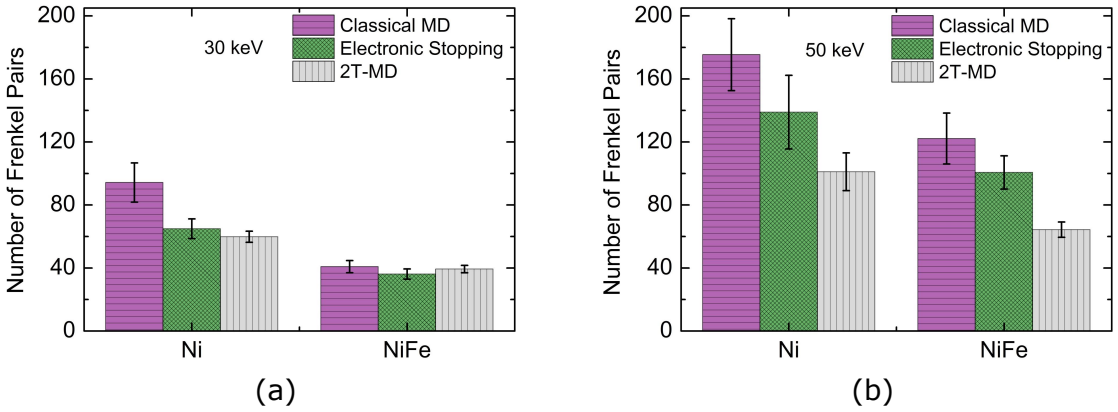

FIG. 1: Average surviving damage at the end of the simulation time for 30 keV ((a)) and 50 keV ((b)) Ni cascades in Ni and NiFe. Results for classical MD simulations, electronic stopping-only simulations and the 2T-MD model are shown, with the standard error over twelve events.

The classical MD simulations of the cascades are performed under the constant volume and energy ensemble (NVE). The electronic effects are included in the friction and 2T-MD model as described previously [6]. The atomic and electronic subsystems in the 2T-MD model simulations are initially in equilibrium, with both the atomic and electronic temperatures being equal to 300 K. For the cascades incorporating electronic stopping, the friction coefficient was calculated using SRIM tables [20] yielding a value of 0.6 ps^{-1} for both systems, and it is applied to atoms with velocity larger than a value that corresponds to double the cohesive energy of the system [21], and is equal to 54 Å ps^{-1}. For the 2T-MD simulations, the e-ph coupling parameters g_p for the two systems were calculated at a temperature equal to 300 K using electronic structure results obtained within the coherent potential approximations [22] (CPA), as described elsewhere [24], and have values of $g_p = 10.85 \times 10^{17}$ W m $^{-3}$ K^{-1} and $g_p = 8.78 \times 10^{17}$ W m $^{-3}$ K^{-1} for Ni and NiFe, respectively. The heat capacity C_e for a range of electron temperatures was calculated using electronic density of states (DOS) obtained from CPA calculations. It should be mentioned that at the temperatures of the interest, in the locally heated areas, both Ni and NiFe are nonmagnetic. Reasoning to this fact, the DOS of nonmagnetic alloys was used for calculation of C_e. The electronic thermal conductivity values for Ni and NiFe are $\kappa_e = 88$ W m^{-1} K^{-1} and 21 W m^{-1} K^{-1}, respectively [25]. No lattice temperature dependence in κ_e is assumed and g_p is considered constant. The value of κ_e decreases with lattice temperature, therefore it is likely to be overestimated in the thermal spike region. A reduced value of electronic thermal conductivity would contribute to the quenching (1 ps) and annealing of the damage (at 1 - 100 ps), which potentially could result in decreased number of point defects.

The e-ph coupling process g_p is activated at 0.2 ps in the simulation time, as the lattice temperature is ill-defined before this. Until this time of the simulation, only the electron stopping mechanism is active. This approximate value was computed by looking at the convergence of kinetic and potential energies (i.e. thermalization) in the friction cascades. The e-ph coupling activation time should be such to allow time for the atoms to thermalize and transfer energy to the electrons. The e-ph switch-on time is a parameter that can affect the electronic and atomic temperature evolution in short times, and therefore can affect the cascade evolution. The thermal diffusion equation is solved across the gridded system volume. Each volume element has an associated electronic temperature. The atomistic temperature is calculated from the kinetic energies that are included in this volume. The electronic grid is extended beyond the system volume to transport energy away from the collision cascades [17]. Each cell has length of about 22 Å and the larger electronic grid consists of $32 \times 32 \times 32$ cells.

In Fig. 1 (a), the average surviving damage based on Wigner-Seitz analysis at the end of the simulation time for each of the three cases for 30 keV Ni irradiation is shown, for Ni and NiFe. As seen here, the electronic stopping for pure Ni results in reduced damage in comparison to the classical MD cascades, but the inclusion of the e-ph interaction does not significantly affect the surviving Frenkel pairs (FP). For NiFe the number of surviving defects is nearly the same for all three simulated models. Similarly, Fig. 1 (b) illustrates the average damage with the standard error over twelve events for 50 keV cascades in Ni and NiFe, for the three simulated models. For this energy, the electronic stopping mechanism in both materials results in decreased damage compared to the classical MD simulations. Additionally, the damage produced when the 2T-MD model is applied is reduced relative to the damage produced in the friction-only cascades. Comparison between Ni and NiFe shows that less damage is produced in NiFe, in agreement with

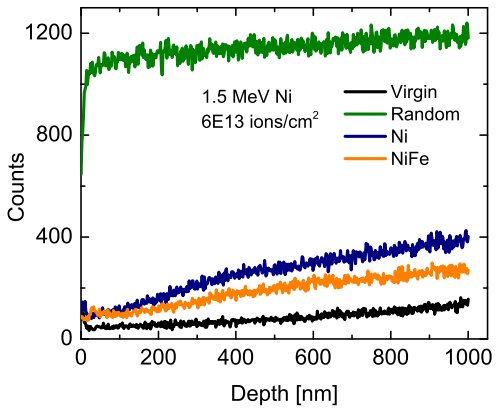

FIG. 2: Relative backscattering yield (count) of Ni and NiFe. The random level indicates unorganized arrangement of atoms (non crystallinity), while the virgin level indicates the defect-free level. The higher yields of Ni and NiFe are attributed to 1.5 MeV Ni ion irradiation a fluence of 6×10^{13} ions/cm^2.

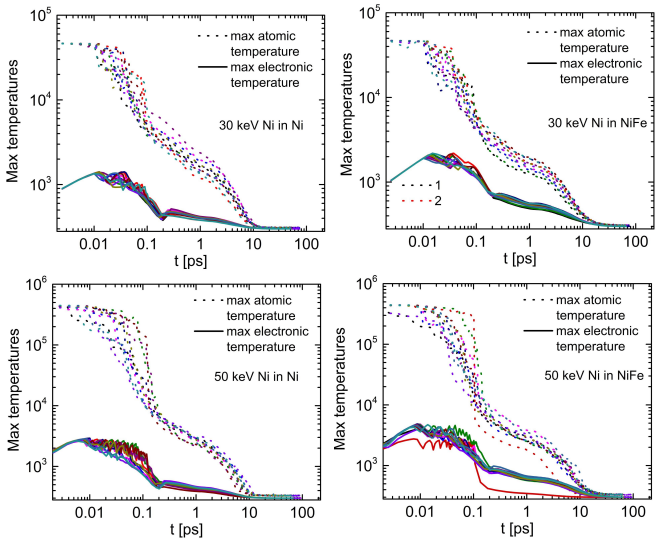

FIG. 3: Maximum per-voxel atomic and electronic temperatures for 30 keV (top) and 50 keV (bottom) Ni 2T-MD cascade simulations in Ni and NiFe for twelve different cascade events. Energy is fed back to the lattice at 0.2 ps and the heat transfer time is about 10 ps for Ni and 11 ps for NiFe, after which the electron–ion temperatures are equilibrated.

recent irradiation experiments [26] and classical MD simulations of lower energy ions and higher fluence in pure nickel and nickel-iron alloys [27].

To validate the modeling results, ion channeling measurements [28] were carried out to compare radiation performance under ion irradiation. In Figure 2 we compare the irradiation resistance from 1.5 MeV Ni ion irradiation in Ni and NiFe with a fuence 6×10^{13} ions/cm^2. Here we see that the relative yield of the damage in Ni is higher than that in NiFe, indicated by the higher yield (count). The MD simulations show that the average damage in Ni is higher than that in NiFe based on the 2T-MD model for both energies. Qualitative agreement between the ion channeling measurements and the MD results is evident.

Figure 3 shows the maximum atomic and electronic temperatures for 30 keV and 50 keV Ni 2T-MD cascades in Ni and NiFe. The maximum electronic temperature is the highest per-voxel value to be found in the grid. We see that the atomic temperature is much higher than the electronic, which indicates that the electronic system acts as a heat sink. Initially, the atomic temperature reaches about 4×10^4 K in 30 keV cascades and 4×10^5 K in 50 keV cascades. At 0.2 ps, energy is fed back to the atomic system and the atomic temperature starts dropping below 1000 - 2000 K. The heat transfer relaxation time, as read from these plots, is about 10 ps for Ni and 11 ps for NiFe, after which the electronic and ionic temperatures are equilibrated. The maximum atomic temperature for the 50 keV Ni irradiation is about 10 times larger than the one for the 30 keV cascades, while the maximum electronic temperature for 50 keV cascades is double the one for 30 keV cascades at short times.

In the 50 keV cascades, higher temperature is developed locally in the cascade due to the higher PKA energy. The electronic stopping, on the one hand, removes energy from the thermal spike, and results in less damage. On the other hand, in the 2T-MD model, energy is fed back to the system via the e-ph coupling, meaning that the cascade cools down slower (slower quenching), and therefore the resulting damage is reduced. While for the lower PKA energy, the electronic effects have a small effect (case of Ni) or nearly no effect (for NiFe); for higher energy, and therefore higher local temperatures, the electronic excitations start affecting the damage production significantly.

Statistics for defect analysis for the simulations of this work are summarized in Table I. The self-interstitial atoms (SIAs) and vacancy clusters are defined using the second nearest-neighbor distance criterion. As mentioned above, quantitatively the electronic effects are more profound in 50 keV cascades than in 30 keV cascades: the friction term in 30 keV Ni cascades results in reduced damage, which is not significantly affected by e-ph coupling; while in the 50 keV cascades, both the friction term and the 2T-MD model result in less damage. Cluster analysis shows that more isolated SIAs and vacancies are produced in Ni for both energies when the friction term is applied. This number increases when the e-ph coupling is included. In NiFe the friction term results in a small decrease in the fraction of isolated defects, which increases when the e-ph coupling is included. Classical MD and 2T-MD simulations give similar values of the fraction of isolated SIAs and vacancies in NiFe, except for the isolated vacancies in the 50 keV cascades, where the value is larger for the 2T-MD. The total number of clusters of size more than 3 found in our simulations does not differ dramatically among the three models for each material and energy, except for the number of vacancy clusters for the higher energy simulations: the number

	Classical MD	Electronic stopping	2T-MD	Classical MD	Electronic stopping	2T-MD
30 keV Ni		**Ni**			**NiFe**	
Number of Frenkel Pairs	94 (12)	65 (6)	60 (4)	41 (4)	36 (3)	40 (2)
Fraction of isolated SIAs	0.11 (0.02)	0.12 (0.02)	0.16 (0.03)	0.40 (0.05)	0.35 (0.05)	0.39 (0.05)
Fraction of isolated vacancies	0.36 (0.04)	0.42 (0.04)	0.56 (0.03)	0.47 (0.05)	0.42 (0.05)	0.48 (0.04)
Number of SIA clusters (containing more than 3 SIAs)	43	33	49	21	19	21
Number of vacancy clusters (containing more than 3 vacancies)	29	29	29	18	20	21
Largest SIA cluster	106	67	41	31	30	33
Largest vacancy cluster	147	57	17	60	40	15
50 keV Ni		**Ni**			**NiFe**	
Number of Frenkel Pairs	175 (23)	139 (23)	101 (12)	122 (16)	100 (11)	64 (5)
Fraction of isolated SIAs	0.08 (0.01)	0.11 (0.02)	0.17 (0.03)	0.40 (0.07)	0.35 (0.04)	0.38 (0.03)
Fraction of isolated vacancies	0.31 (0.05)	0.37 (0.05)	0.55 (0.05)	0.42 (0.07)	0.39 (0.03)	0.50 (0.03)
Number of SIA clusters (containing more than 3 SIAs)	67	78	67	44	53	41
Number of vacancy clusters (containing more than 3 SIAs)	80	41	36	40	54	26
Largest SIA cluster	136	112	66	136	41	31
Largest vacancy cluster	244	292	129	118	85	31

TABLE I: Defect number and cluster analysis statistics for 30 keV and 50 keV Ni cascades in Ni and NiFe, with the standard error of the mean calculated over twelve events. The cluster statistics refer to clusters with size more than 3, i.e. containing four or more SIAs or vacancies. The clusters are determined by net defect count (difference between the number of SIAs and the number of vacancies). The largest clusters found in each set of twelve simulations are presented in the last row.

of vacancy clusters produced in 50 keV Ni 2T-MD cascades in Ni and NiFe is nearly half of that created in the classical MD simulations. The largest SIA and vacancy clusters found in each set of simulations are also provided.

Overall in the 2T-MD model there is less damage, smaller fraction of isolated point defects and an insignificant difference in the number of clusters in comparison to the classical MD simulations, meaning that smaller clusters are produced. The 2T-MD model results in fewer vacancy clusters for 50 keV cascade events. Figure 4 shows the surviving interstitials and vacancies of a representative 50 keV Ni classical MD cascade and a representative 50 keV Ni 2T-MD cascade in NiFe for the same direction of the PKA. We can easily distinguish more isolated point defects and smaller defect clusters in the 2T-MD cascades. Generally, in addition to the reduced damage in NiFe than in Ni, less SIA and vacancy clusters, as well as more isolated defects, are formed in NiFe under each simulation condition.

In summary, we presented quantitative and qualitative comparison of the produced damage in 30 and 50 keV Ni cascades in Ni and NiFe for classical MD simulations and simulations where we take the electronic effects into account, and comparison with experimental results. We find that the electronic effects are more profound for

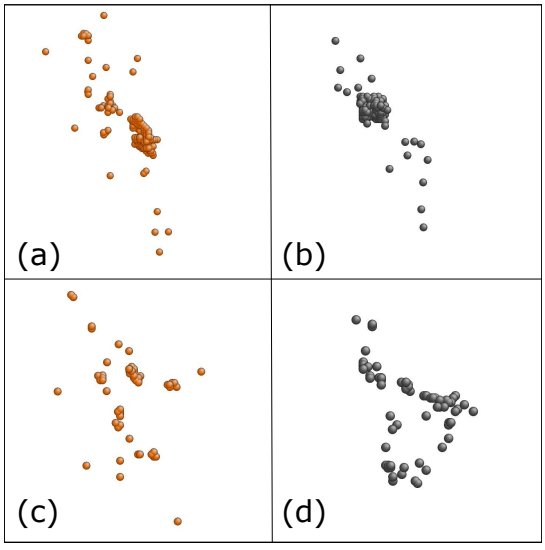

FIG. 4: The final damage of a representative 50 keV classical MD cascade (top) and a representative 50 keV 2T-MD cascade (bottom) in NiFe is shown, for the same PKA velocity direction. (a) and (c) show the surviving interstitials and (b) and (d) show the surviving vacancies. The frames shown have size 196 Å×196 Å×196 Å.

the higher energy events and the energy returned to the lattice via the e-ph interactions enhances defect recombination. Additionally more isolated defects are produced when the 2T-MD model is applied. Our results demonstrate the need to include a model to describe the e-ph coupling in a local way, as it can affect the damage level and the defect distribution into clusters, which are of great importance in the resistance to radiation as they can affect the materials' properties and long term performance. The resulting configurations of the simulations of this work could be used in further investigation of the three irradiation conditions regarding the damage evolution in larger timescales with the used of accelerated dynamics. Further investigation of the electronic effects in more alloys and at higher energies is needed in order to obtain fundamental understanding of radiation damage and investigate how the electronic excitations in combination with alloy complexity affect the materials' behavior in extreme conditions. Additionally, further development of the model parameters will enable more accurate and realistic approximations of the radiation effects.

This work was supported by Energy Dissipation to Defect Evolution (EDDE), an Energy Frontier Research Center funded by the U.S. Department of Energy, Office of Science, Basic Energy Sciences. We appreciate the scientific discussions and interpretation of the experimental results with Yanwen Zhang at ORNL. We thank Ke Jin, ORNL, for polishing the sample surface suitable for the ion channeling measurements. The simulation used resources of the National Energy Research Scientific Computing Center, supported by the Office of Science, US Department of Energy, under Contract No. DEAC02-05CH11231.

[1] K. Nordlund and R.S. Averback, Phys. Rev. B 56 (1997) 2421.
[2] K. Trachenko, M. T. Dove, E. Artacho, I. T. Todorov, W. Smith, Phys. Rev. B 73 (2006) 174207.
[3] 1.11-primary radiation damage formation, in: R.J. Konings (Ed.), Comprehensive Nuclear Materials, Elsevier, Oxford, 2012, pp. 293-332.
[4] K. Trachenko, E. Zarkadoula, I.T. Todorov, M.T. Dove, D.J. Dunstan, K. Nordlund, Nucl. Instr. Meth. B 277 (2012) 613.
[5] E. Zarkadoula et al., J. Phys.: Condens. Mat. 25 (2013) 125402.
[6] E. Zarkadoula et al., J. Phys.: Condens. Matter 26 (2014) 085401.
[7] E. Zarkadoula, D. M. Duffy, K. Nordlund, M. A. Seaton, I. T. Todorov, W. J. Weber, and K Trachenko: *J. Phys.: Condens. Matter* 27 (2015) 135401.
[8] O.N. Senkov, G.B. Wilks, D.B. Miracle, C.P. Chuang, P.K. Liaw, Intermetallics 18 (2010) 1758.
[9] M.H. Chuang, M.H. Tsai, W.R. Wang, S.J. Lin, J.W. Yeh, Acta Mater 59 (2011) 6308.
[10] S.G. Ma, Y. Zhang, Mat. Sci. Eng. A 532 (2012) 480.
[11] Y. Zhang, T.T. Zuo, Z. Tang, M.C. Gao, K.A. Dahmen, P.K. Liaw, et al., Prog. Mater. Sci. 61 (2014) 1.
[12] Z. Wu, H. Bei, G.M. Pharr, E.P. George, Acta Mater. 81 (2014) 428.
[13] Z. Wu, H. Bei, F. Otto, G.M. Pharr, E.P. George, Intermetallics 46 (2014) 131.
[14] B. Gludovatz, A. Hohenwarter, D. Catoor, E.H. Chang, E.P. George, R.O. Ritchie, Science 345 (2014) 1153-1158.
[15] I. T. Todorov, B. Smith, M. T. Dove and K. Trachenko, J. Mater. Chem. **16**, 1911 (2006).
[16] D. M. Duffy and A. M. Rutherford, J. Phys.: Condens. Mat. 19 (2007) 016207.
[17] A. M. Rutherford and D. M. Duffy, J. Phys.: Condens. Mat. 19 (2007) 496201.
[18] L. Kantorovich and N. Rompotis, Phys. Rev. B 78 (2008) 094305.
[19] G. Bonny, N. Castin, D. Terentyev, Model. Simul. Mater. Sci. Eng. 21 (2013) 85004.
[20] http://www.srim.org/
[21] E. Zhurkin and A. Kolesnikov, Nucl. Instr. Methods Phys. Res., Sect. B, 202 (2003) 269–277.
[22] P. Soven. Phys. Rev. 156 (1967) 809.
[23] D. W. Taylor. Phys. Rev. 156 (1967) 1017.
[24] G. D. Samolyuk, L. K. Béland, G. M. Stocks, and R. E. Stoller, J. Phys.: Condens. Mat., 28 (2016) 175501.
[25] K. Jin, B. C. Sales, G. M. Stocks, G. D. Samolyuk, M. Daene, W. J. Weber, Y. Zhang and H. Bei, Sci. Rep. 6 (2016) 20159.
[26] Y. Zhang, G.M. Stocks, K. Jin, C. Lu, H. Bei, B.C. Sales, L. Wang, L.K. Béland, R.E. Stoller, G.D. Samolyuk, M. Caro, A. Caro, W.J. Weber, Nat. Commun. 6 (2015) 8736.
[27] M.W. Ullah, D. S. Aidhy, Y. Zhang, W. J. Weber, Acta Materialia 109 (2016) 17-22.
[28] Y. Zhang, M.L. Crespillo, H. Xue, K. Jin, C.H. Chen, C.L. Fontana, J.T. Graham, W.J. Weber, Nucl. Instr. Methods Phys. Res., Sect. B 338 (2014) 1930.